EPJ A
Hadrons and Nuclei

EPJ.org
your physics journal

Eur. Phys. J. A **42**, 105–110 (2009) DOI: 10.1140/epja/i2009-10850-2

Dynamic potential barrier in the entrance phase of heavy-ion fusion reactions

J.-L. Tian, X. Li, X.-Z. Wu, Z.-X. Li and S.-W. Yan

EDP SCIENCES Società Italiana di Fisica Springer

Eur. Phys. J. A **42**, 105–110 (2009)
DOI 10.1140/epja/i2009-10850-2

THE EUROPEAN PHYSICAL JOURNAL A

Regular Article – Theoretical Physics

Dynamic potential barrier in the entrance phase of heavy-ion fusion reactions

J.-L. Tian[1,2,a], X. Li[1], X.-Z. Wu[2], Z.-X. Li[2], and S.-W. Yan[1]

[1] College of Nuclear Science and Technology, Beijing Normal University, Beijing 100875, PRC
[2] China Institute of Atomic Energy, Beijing 102413, PRC

Received: 20 March 2009 / Revised: 5 July 2009
Published online: 2 August 2009 –
Communicated by T.S. Bíró

Abstract. Based on the improved quantum molecular-dynamics (ImQMD) model, the incident energy dependence of dynamic potential barriers is investigated in the entrance channel of fusion reactions. The height of the dynamic barrier increases with the incident energy at energies around the Coulomb barrier. The calculated lowest dynamic barrier approaches to the adiabatic barrier, while the highest one goes up to the sudden potential barrier. To understand the energy dependence of the dynamical barrier we study the neck formation and shape evolution of the system which causes the dynamic lowering of the barrier.

PACS. 25.70.-z Low and intermediate energy heavy-ion reactions – 24.10.-i Nuclear reaction models and methods

Being encouraged by the synthesis of superheavy elements (SHEs), the investigation of fusion mechanism at energies around the Coulomb barrier has recently received a great attention theoretically and experimentally [1–5]. However, up to now [6] the mechanism of the compound-nucleus formation in the fusion of heavy nuclei near the Coulomb barrier is still far from clear. Several models are proposed to describe the dynamical mechanism of the fusion reaction. One is called dinuclear system (DNS) concept [7,8] in which the fusion happens in the mass asymmetry coordinate by the transfer of a series of nucleon or small cluster from a light nucleus to a heavier one at the touching configuration or the DNS decays by quasifission. In another type [9–12] the fusion occurs along the radial coordinate using adiabatic potential energy surface (PES) obtained either with the liquid-drop model or Strutinsky's macroscopic-microscopic method. The DNS model assumes a sudden potential energy surface in the radial coordinate, while the PES behaves adiabatically along the fusion path in the mass asymmetry coordinate. Although two sorts of models have been used to explain many experimental evaporation residues cross-sections, their theoretical foundations are still not clear enough, yet. Recently, a new model [13,14] that includes the time-dependent dynamics of the single-particle motion in conjunction with the macroscopic evolution of the system is proposed, and it describes that the gradual transition from the diabatic to the adiabatic potential energy surface leads to fusion or quasifission. In this work, the frozen density potential and the adiabatic potential are also discussed in the entrance phase of heavy-ion fusion reactions.

In the process of heavy-ion fusion reaction, the interaction of two colliding nuclei consists of an attractive nuclear potential and a repulsive Coulomb potential. This creates a Coulomb barrier which the system has to overcome in order to fuse. The interacting potential between nuclei plays an important role in the description of most heavy-ion reactions, since the fusion cross-section mainly depends on the height and position of the Coulomb barrier [15]. However, in the calculations, we find that the Coulomb barrier is energy dependent. This dependence is also discussed in the time-dependent Hartree Fock (TDHF) calculations [16]. We try to find the dynamical behavior of the fusion barrier, the lowest dynamical barrier (which is very close to the adiabatic barrier) and the upper limit of the dynamical barrier (which approaches to the frozen density barrier). In the present work, both the static barrier based on the frozen density approximation and the incident-energy–dependent fusion potential barrier are microscopically calculated using the improved quantum molecular-dynamics (ImQMD) model [17,18]. The quantum molecular-dynamics (QMD) model being widely used in intermediate-energy heavy-ion collisions was successfully extended to heavy-ion collisions at energies near barrier by making a series improvements [17,18]. The main improvements introduced are as follows: the surface and surface symmetry energy terms are introduced in the potential energy density functional in the mean field; a sys-

[a] e-mail: tianjl@bnu.edu.cn

tem size-dependent wave packet width is introduced; an approximate treatment of anti-symmetrization, namely, the phase space occupation constrain is adopted [19]. The initial nuclei for projectile and target are sampled according to the density, binding energy and root-mean-square radius of nuclei, which are obtained from calculation of mean-field theory or experimental data. By using this microscopic dynamic model, the motions such as shape deformations, neck formation and rupture, nucleon transfer and so on are involved consistently. With the ImQMD model the fusion dynamics at energies near and above the barrier has extensively been studied and can reproduce a series of experimental data [17,18,20,21].

In the ImQMD model, each nucleon is represented by a coherent state of a Gaussian wave packet. Through a Wigner transformation, the one-body phase space distribution function for N-distinguishable particles is given by

$$f(\mathbf{r},\mathbf{p})=\sum_i \frac{1}{(\pi\hbar)^3}\exp\left[-\frac{(\mathbf{r}-\mathbf{r}_i)^2}{2\sigma_r^2}-\frac{2\sigma_r^2}{\hbar^2}(\mathbf{p}-\mathbf{p}_i)^2\right]. \quad (1)$$

Here $\mathbf{r}_i$ and $\mathbf{p}_i$ are the centers of the i-th wave packet in the coordinate and momentum space, respectively. σ_r represents the spatial spread of the wave packet. For identical fermions, the effects of the Pauli principle were discussed in a broader context by Feldmeier and Schnack [22]. The approximate treatment of anti-symmetrization is adopted in the ImQMD model by means of the phase space occupation constraint method [19]. The density and momentum distribution functions of a system read

$$\rho(\mathbf{r})=\int f(\mathbf{r},\mathbf{p})\mathrm{d}^3p=\sum_i \frac{1}{(2\pi\sigma_r^2)^{3/2}}\exp\left[-\frac{(\mathbf{r}-\mathbf{r}_i)^2}{2\sigma_r^2}\right], \quad (2)$$

$$g(\mathbf{p})=\int f(\mathbf{r},\mathbf{p})\mathrm{d}^3r=\sum_i \frac{1}{(2\pi\sigma_p^2)^{3/2}}\exp\left[-\frac{(\mathbf{p}-\mathbf{p}_i)^2}{2\sigma_p^2}\right], \quad (3)$$

respectively, where the sum runs over all particles in the system. And σ_r and σ_p satisfy the minimum uncertainty relation

$$\sigma_r\cdot\sigma_p=\frac{\hbar}{2}. \quad (4)$$

Considering the fact that for a finite system the nucleons are localized in a finite region corresponding to the size of the system, the width of the wave packet representing nucleons in the system should have a relation with the size of the system. As the same as ref. [17], we adopt a system size-dependent wave packet width $\sigma_r=0.16N^{1/3}+0.49$, where N is the number of nucleons bound in the system.

The propagation of nucleons under the self-consistently generated mean field is governed by Hamiltonian equations of motion:

$$\dot{\mathbf{r}}_i=\frac{\partial H}{\partial\mathbf{p}_i}, \qquad \dot{\mathbf{p}}_i=-\frac{\partial H}{\partial\mathbf{r}_i}. \quad (5)$$

The Hamiltonian H consists of the kinetic energy and the effective interaction potential energy:

$$H=T+U, \quad (6)$$

$$T=\sum_i\frac{p_i^2}{2m}. \quad (7)$$

The effective interaction potential energy includes the nuclear local interaction potential energy and the Coulomb interaction potential energy:

$$U=U_{loc}+U_{coul}. \quad (8)$$

and

$$U_{loc}=\int V_{loc}\mathrm{d}^3r. \quad (9)$$

Here V_{loc} is the potential energy density.

The potential energy density V_{loc} in the ImQMD model reads

$$V_{loc}=\frac{\alpha}{2}\frac{\rho^2}{\rho_0}+\frac{\beta}{\gamma+1}\frac{\rho^{\gamma+1}}{\rho_0^\gamma}+\frac{g_0}{2\rho_0}(\nabla\rho)^2+g_\tau\frac{\rho^{\eta+1}}{\rho_0^\eta}+\frac{C_s}{2\rho_0}(\rho^2-\kappa_s(\nabla\rho)^2)\delta^2, \quad (10)$$

where the $\delta=(\rho_n-\rho_p)/(\rho_n+\rho_p)$ is the isospin asymmetry. The first three terms in the above expression can be obtained from the Skyrme energy density functional directly. The fifth term is the symmetry potential energy part which includes both the bulk and the surface symmetry energy terms. In addition, we introduce an extra small correction term $V_\tau=g_\tau\frac{\rho^{\eta+1}}{\rho_0^\eta}$ (named τ term) in the potential energy functional. Inserting expression (10) into (9), we obtain the local interaction potential energy omitting self-energies:

$$U_{loc}=\frac{\alpha}{2}\sum_i\sum_{j\neq i}\frac{\rho_{ij}}{\rho_0}+\frac{\beta}{\gamma+1}\sum_i\left(\sum_{j\neq i}\frac{\rho_{ij}}{\rho_0}\right)^\gamma+\frac{g_0}{2}\sum_i\sum_{j\neq i}f_{sij}\frac{\rho_{ij}}{\rho_0}+g_\tau\sum_i\left(\sum_{j\neq i}\frac{\rho_{ij}}{\rho_0}\right)^\eta+\frac{C_s}{2}\sum_i\sum_{j\neq i}t_it_j\frac{\rho_{ij}}{\rho_0}(1-\kappa_sf_{sij}), \quad (11)$$

where

$$\rho_{ij}=\frac{1}{(4\pi\sigma_r^2)^{3/2}}\exp\left[-\frac{(\mathbf{r}_i-\mathbf{r}_j)^2}{4\sigma_r^2}\right], \quad (12)$$

$$f_{sij}=\frac{3}{2\sigma_r^2}-\left(\frac{\mathbf{r}_i-\mathbf{r}_j}{2\sigma_r^2}\right)^2, \quad (13)$$

and $t_i=1$ and -1 for the proton and the neutron, respectively. $r_{ij}=|r_i-r_j|$ is the relative distance. One should note that the third term in eq. (11) comes from both the surface term and the correction to the second term of eq. (10) (see ref. [17]), and thus g_0 is actually treated as a parameter in this model.

Table 1. The model parameters IQ1.

α (MeV)	β (MeV)	γ	g_0 (MeV fm^2)	g_τ (MeV)	η	C_S (MeV)	κ_s (fm^2)	ρ_0 (fm^{-3})
−310.0	258.0	7/6	19.8	9.5	2/3	32.0	0.08	0.165

The Coulomb energy can be written as a sum of the direct and the exchange contribution, and the latter being taken into account in the Slater approximation [23]

$$U_{coul} = \frac{e^2}{2}\int \frac{\rho_p(\mathbf{r})\rho_p(\mathbf{r}')}{|\mathbf{r}-\mathbf{r}'|}\mathrm{d}\mathbf{r}\mathrm{d}\mathbf{r}' - e^2\frac{3}{4}\left(\frac{3}{\pi}\right)^{1/3}\int \rho_p^{4/3}\mathrm{d}\mathbf{r}, \tag{14}$$

where ρ_p is the density distribution of protons of the system. The collision term and phase space occupation constraint can also re-adjust the momenta, but the former plays a very small role in low-energy heavy-ion collisions and the latter only happens occasionally.

By this model with the fixed set of parameters IQ1 (see table 1), the properties of the nuclear ground state (binding energies and the root-mean-square radii) and the fusion reactions between light and intermediate heavy nuclei can be described well [17,18], and the capture cross-sections of massive nuclear systems and the charge distributions of products in the central collision of very massive systems, for example, the Ca + Ca and Xe + Sn are also reproduced very well [18]. Now let us apply the model to study the dynamic barrier in the heavy-ion fusion reaction of ^{86}Kr + ^{100}Mo head-on collisions. The initial nuclei of the projectile and target are prepared by the same procedure as that in refs. [17,18].

The interaction potential $V_b(R)$ between reaction partners can be written as

$$V_b(R) = E_{12}(R) - E_1 - E_2. \tag{15}$$

where R is the center-to-center distance between projectile and target, which is a function of time. $E_{12}(R)$, E_1 and E_2 are the total energy of the whole system, the energies of the projectile-like and the target-like part, which are the integration of time-dependent energy density functional over the whole system, the projectile-like and the target-like, respectively. The potential energy functional is given by formula (11) and for the kinetic energy density functional the Thomas-Fermi approximation is adopted as mentioned in ref. [24]. The collective kinetic energy has already been subtracted in expression (15) by using eqs. (6) and (7). By using the ImQMD model, both the static and dynamic potential barrier can be calculated. For the calculation of the static Coulomb barriers, the static density distribution, which is the same as the initial density distribution of the projectile and target, is adopted, while for the dynamic Coulomb barrier case the density distribution of the system changes dynamically due to the interaction between the reaction partners.

In the fusion process, we can calculate the contour plot of the density distribution of the system at each time step for each event by using the ImQMD model. The schematic picture in fig. 1 illustrates the shape of the system for a typical head-on collision event at the initial period of neck formation. The shape is determined by the contour map with the density equal to 0.02/fm^3. Some geometry quantities are showed in fig. 1. R denotes the center-to-center distance between projectile (or projectile-like) and target (or target-like), Δ and L denote the neck radius and the elongation of the total system. The points denoted by index 1 and 2 are the center of the projectile (or projectile-like) and of the target (or target-like), respectively. To explore the dynamic barrier, we must give the specific definitions of the projectile-like and target-like. When the neck is formed, we first determine the minimum point O of the contour plot of the density distribution along the line through 1 and 2, then we find out the perpendicular line of CD, which goes through the O point in the plane xoz. A and B are the cross points of the perpendicular line and surface of the system. AB is the neck radius of the system, and its size is denoted by Δ. In order to apply formula (15), the left part on AB is regarded as projectile-like and the right part on AB is regarded as target-like. The neck grows up with time evolution. When the neck disappears, the dinuclear system turns into a strongly deformed mononucleus compound system, and the formula (15) is not suitable for describing the barrier anymore. At that time, the distance of the two centers becomes very small and the potential is far away from the dynamic barrier. So we do not need to distinguish the projectile-like and target-like parts.

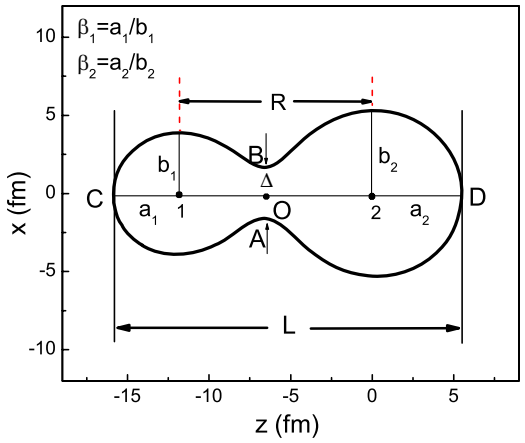

Fig. 1. The definition of some geometrical quantities related to the nuclear shape.

Now we present the numerical results of the dynamic (and static) potential barrier for the head-on fusion reaction of ^{86}Kr + ^{100}Mo in fig. 2. The crossed and dotted curves denote the proximity potential from ref. [25] and the static potential. Here the static potential is obtained with the density frozen approximation. The line with open

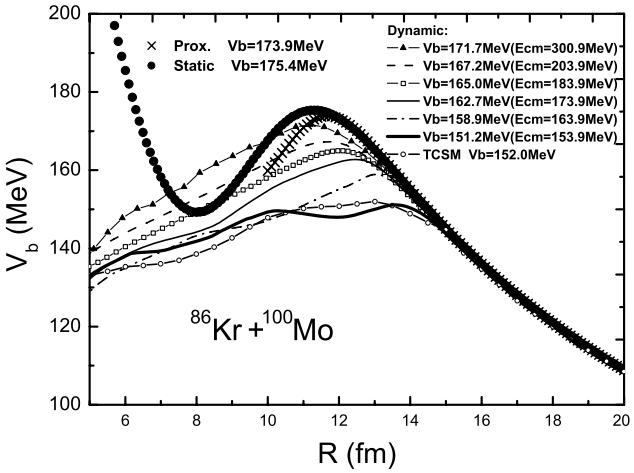

Fig. 2. The potential barrier as a function of the center-to-center distance between the nuclei for a head-on collision of ^{86}Kr + ^{100}Mo. The dotted and crossed curves are for the static and proximity potential, respectively. The line with empty circles is from Stutinsky's macroscopic-microscopic calculation based on the two-center shell model. The other six lines from up to down are for dynamic potentials at incident energies E_{cm} = 300.9, 203.9, 183.9, 173.9, 163.9 and 153.9 MeV, respectively.

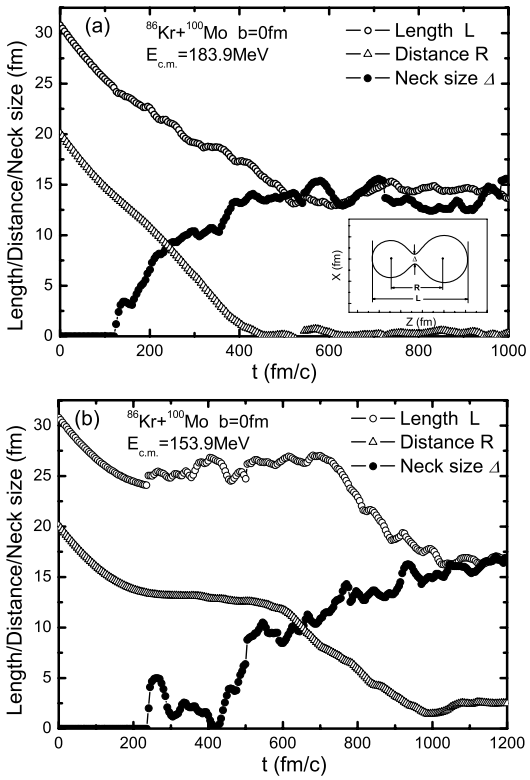

Fig. 3. The time evolution of the elongation (open circles), the center-to-center distance of two fragments (open triangles), and the neck size (full circles) of the composite system in the fusion reaction ^{86}Kr + ^{100}Mo. Panels (a) and (b) show incident energies 10 MeV above and 20 MeV below the static barrier (proximity potential barrier), respectively.

circles denotes the adiabatic potential barrier, which is calculated by Strutinsky's macroscopic-microscopic method based on the two-center shell model [26,27] in which the liquid-drop energy plus the shell correction are considered. The shape parameters used in the calculation of the adiabatic potential vary with the distance R between projectile and target and they are determined from the ImQMD model calculation by the method of the fixed equidensity surface at $\rho = 0.3\rho_0$. The lines with full triangles, the dashed line, the open square, the thin solid line, the dot-dashed line and the thick line are all for dynamic potentials at incident energies E_{cm} = 300.9, 203.9, 183.9, 173.9, 163.9 and 153.9 MeV, respectively. It is clear that, in general, $V_b(R)$ is a function of time since the density distribution of the reaction system changes with time. Only in a static case, the density distribution of projectile and target is always assumed to be the same as that at the initial time. In this case the dynamical effects experienced by fusion partners during the reaction process are not taken into account. One can see from the figure that the value of our static barrier is quite close to that of the well-known proximity potential barrier. However, for the realistic fusion reactions the density distributions of the projectile and of the target change with time under the influence of the mean field, and the shape of the fusion system and their neck evolve with time. Therefore, the dynamical potential should strongly depend on the incident energy (as well as impact parameter) for a certain reaction system. We define the maximal value of the dynamic potential (experienced in the path of fusion) as the height of the dynamic potential barrier. From the dynamic calculation one can see that when the incident energy is quite high, for example, E_{cm} = 300.9 MeV, the dynamical barrier reaches $V_b(R)$ = 171.7 MeV which is close to the static barrier $V_b(R)$ = 173.9 MeV. With the decrease of the incident energy, the height of the barrier decreases. For example, at E_{cm} = 173.9 MeV the dynamical barrier reduces to $V_b(R)$ = 162.7 MeV. When the incident energy goes down to much below the static barrier, for instance, at E_{cm} = 153.9 MeV, the dynamical barrier further decreases to $V_b(R)$ = 151.2 MeV which approaches to the adiabatic static barrier ($V_b(R)$ = 152.0 MeV). From the above studies we can obtain the following conclusions: 1) the dynamical barriers are incident energy dependent, and the larger the incident energy, the higher the dynamic barrier. 2) With increasing entrance energy, the dynamic barrier goes towards the frozen density barrier. 3) One can find that the lowest dynamic barrier is very close to the adiabatic potential barrier calculated by Strutinsky's macroscopic-microscopic method.

To understand the energy dependence of the dynamic barrier, we study the neck dynamics and change of shape for the fusion system ^{86}Kr + ^{100}Mo. In fig. 3 we show the time evolution of the neck size (line with full circles), the center-to-center distance between the two fragments (line with empty triangles), and the total length of the fusing system along the reaction axis (line with open circles). Panels (a) and (b) show incident energies 10 MeV above and 20 MeV below the static barrier

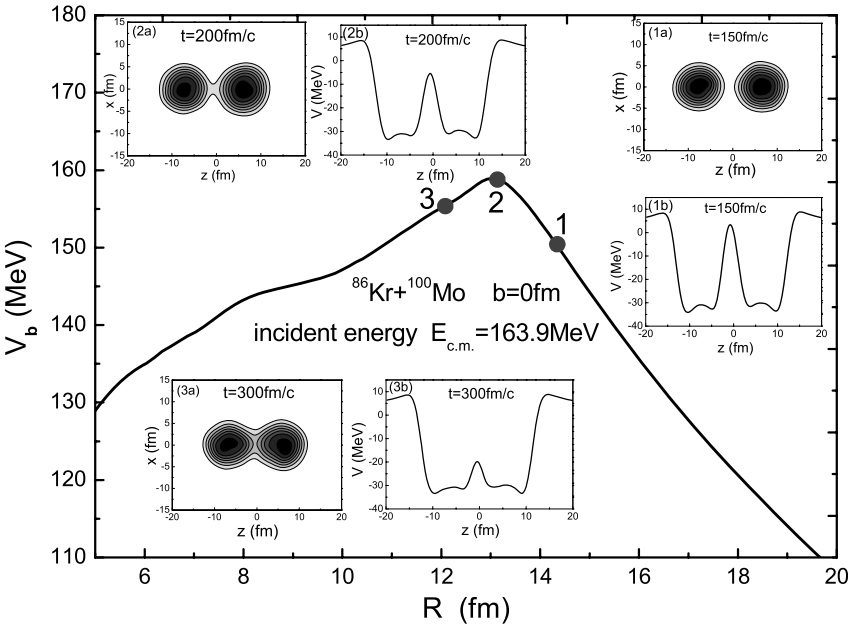

Fig. 4. The fusion path for a head-on collision of $^{86}\mathrm{Kr} + {}^{100}\mathrm{Mo}$ at an energy 10 MeV below the Coulomb barrier. Insets (1a), (2a), (3a) are the contour plots of the density distributions at different times: $t = 150$, 200, 300 fm/c, respectively, and (1b), (2b), (3b) are the corresponding single-particle potentials at different times: $t = 150$, 200, 300 fm/c, respectively.

(proximity potential barrier), respectively. From fig. 3 one can see that for the case of the incident energy much below the static barrier, the neck formation seems to be later than that of the energy above the static barrier, and in the former case the neck size starts to increase from a time of about 220 fm/c and then decreases, even vanishes, then increases again. The neck size oscillates during the time from 220 fm/c to 420 fm/c. This vibration of the neck size makes the fusing system stay at touching configuration for a longer period of time, which results in the fact that the center-to-center distance between the two fragments almost stops to decrease with time in this period and the fusing system has enough time to re-adjust the shape of the system which is energetically favorable and is close to the adiabatic case. In this way, the total length of the fusion system is larger than that of the energy above the static barrier. Therefore, we obtain that the dynamic barrier at $E_{c.m.} = 153.9$ MeV is lower than that at $E_{c.m.} = 183.9$ MeV.

For further investigating the fusion dynamics, we pay a special attention to study the configuration along the fusion path in the fusion potential energy surface. As an example, in fig. 4 we illustrate one typical fusion event of the head-on fusion reaction of $^{86}\mathrm{Kr} + {}^{100}$ Mo at an energy 10 MeV below the barrier. In the figure we plot the dynamic barrier V_b as a function of the center-to-center distance. Simultaneously, in the insets we plot the contour plots of density distributions as well as the corresponding single-particle potentials at 3 typical times, *i.e.*, before, at, and after reaching the highest value of the dynamic barrier along the fusion path. The single-particle potential is calculated by

$$V_{sp}(\mathbf{r}) = \int \rho(\mathbf{r}')V(\mathbf{r} - \mathbf{r}')\mathrm{d}\mathbf{r}', \qquad (16)$$

with $\rho(\mathbf{r})$ being the density distribution of the system and $V(\mathbf{r} - \mathbf{r}')$ the effective nucleon-nucleon interaction. Insets (1a) and (1b) are the contour plots of the density distribution as well as the corresponding single-particle potential at point 1 of the fusion path. One can see from these two figures that at this point the fusion partners are not in touch (see inset (1a)), and there is a high enough inner potential barrier which prevents nucleons from moving from the projectile to the target, or viceversa (see inset (1b)). At the time, corresponding to the point 2, the dynamic barrier reaches a maximal value. The contour plot of the density distribution (inset (2a)) shows that the fusion partners are at a touching configuration, a neck starts to grow, and following this, the inner potential barrier in the potential well is reduced, allowing a few nucleons to move from the projectile to the target, or viceversa (inset (2b)). At the time corresponding to point 3, the dynamical barrier is reduced considerably. Insets (3a) and (3b) show that the neck develops considerably at this moment and, consequently, the inner potential barrier in the potential well is reduced substantially, and the nucleon transfer between the projectile and the target becomes much easier than before. This means that a pre-compound nucleus starts to be formed. From this study we have learned how the dynamical fusion barrier is correlated with the development of the configuration of fusion partner along the fusion path. Associating the single-particle potentials obtained at different stages of fusion with the two-center shell model [26], we can study the time evolution of the single-particle states of the fusion system in the configuration space of single-particle orbits along the fusion path, by which one can study the collectivization of nucleons [1] quantitatively. This kind of work is in progress.

In summary, within the improved quantum molecular-dynamics model we have studied the incident-energy–dependent potential barrier of fusion systems. In our approach the fusion barrier based on the initial density of the system and the frozen density approximation is called the static barrier. The real dynamical barrier encountered in the fusion process strongly depends on the incident energy. The height of dynamical barrier decreases with the decrease of the incident energy, and finally approaches a value which is close to the adiabatic barrier calculated by Strutinsky's macroscopic-microscopic method. With increasing incident energy the dynamic barrier increases and approaches to the static barrier. We also find that the neck formation and shape evolution of the fusion process mainly cause the lowering of the dynamic barrier. In the ImQMD model both the nuclear mean field and collision term allowing for nucleon-nucleon scattering are treated properly, other effects (*i.e.*, shell and parity effects, etc.) are completely ignored in our calculation. On the other hand, the anti-symmetrization between the nucleons plays a very important role in the collision. It is approximately treated in the ImQMD model by the phase space occupation constraint method, which partly made up for its lack of fermionic nature. Due to the approximate treatment of the anti-symmetrization and ignoring the shell effects, the ImQMD model can only provide an approximate internuclear potential in fusion reactions. To obtain a more accurate dynamic potential barrier, one needs to improve the model further.

One of the authors (J.L. Tian) is grateful to Dr. M. Liu for fruitful discussions, and Prof. N. Wang for a careful reading of the manuscript and useful suggestions. This work is partly supported by the National Natural Science Foundation of China (Nos. 10475008, 10875031 and 10675172) and the Scientific Research Foundation for the Returned Overseas Chinese Scholars, Ministry of Personnel and Ministry of Education of China (MOP2006138). The numerical simulation of this research is supported by the HSCC of Beijing Normal University.

References

1. V.I. Zagrebaev, Phys. Rev. C **64**, 034606 (2001).
2. A. Diaz-Torres, G.G. Adamian, N.V. Antonebko, W. Scheid, Phys. Lett. B **481**, 228 (2000).
3. G.G. Adamian, N.V. Antonebko, A. Diaz-Torres, W. Scheid, Nucl. Phys. A **671**, 233 (2000).
4. Y. Aritomo, T. Wada, M. Ohta, Y. Abe, Phys. Rev. C **59**, 796 (1999).
5. C. Shen, G. Kosenko, Y. Abe, Phys. Rev. C **66**, 061602(R) (2002).
6. Rostislav Jolos, Werner Scheid (Editors), *Proceedings of the Symposium on Nuclear Clusters* (EP Systema, Debrecen, Hungary, 2003).
7. N.V. Antonenko, E.A. Cherepanov, A.K. Nasirov, V.P. Permjakov, V.V. Volkov, Phys. Lett. B **319**, 425 (1993); Phys. Rev. C **51**, 2635 (1995).
8. G.G. Adamian, N.V. Antonebko, W. Scheid, Nucl. Phys. A **618**, 179 (1997); **627**, 361 (1997); **678**, 24 (2000); Phys. Rev. C **68**, 034601 (2003).
9. W.J. Swiatecki, Nucl. Phys. A **376**, 275 (1982).
10. G. Royer, B. Remaud, Nucl. Phys. A **444**, 477 (1985).
11. Y. Abe *et al.*, Acta Phys. Pol. B **34**, 2091 (2003).
12. Y. Abe, C.W. Shen, G. Kosenko, in *Nonequilibrium and Nonlinear Dynamics in Nuclear and Other Finite Systems, Beijing 2001*, edited by Z. Li, K. Wu, E. Zhao, F. Sakata, AIP Conf. Proc. **597**, 209 (2001).
13. A. Diaz-Torres, Phys. Rev. C **69**, 021603(R) (2004).
14. A. Diaz-Torres, Phys. Rev. C **74**, 064601 (2006).
15. C.Y Wong, Phys. Rev. Lett. C **31**, 766 (1973).
16. K. Washiyama, D. Lacroix, Phys. Rev. C **78**, 024610 (2008).
17. N. Wang, Z.X. Li, X.Z. Wu, Phys. Rev. C **65**, 064608 (2002).
18. N. Wang, Z.X. Li, X.Z. Wu *et al.*, Phys. Rev. C **69**, 034608 (2004).
19. M. Papa, T. Maruyama, A. Bonasera, Phys. Rev. C **64**, 024612 (2001).
20. N. Wang, Z.X. Li, X.Z. Wu, E.G. Zhao, Mod. Phys. Lett. A **20**, 2619 (2005).
21. J.L. Tian, X.Z. Wu, Z.X. Li *et al.*, Phys. Rev. C **77**, 064603 (2008).
22. H. Feldmeier, J. Schnack, Rev. Mod. Phys. **72**, 655 (2000).
23. J.C. Slater, Phys. Rev. **81**, 85 (1951).
24. M. Brack, C. Guet, H.B. Hakanson, Phys. Rep. **123**, 275 (1985).
25. W.D. Myers, W.J. Swiatecki, Phys. Rev. C **62**, 044610 (2000).
26. J.A. Maruhn, W. Greiner, Z. Phys. **251**, 431 (1972).
27. Xizhen Wu, J.A. Maruhn, W. Greiner, Z. Phys. A **334**, 207 (1989).